

Quantum Mechanics/Molecular Mechanics Studies on the Sulfoxidation of Dimethyl Sulfide by Compound I and Compound 0 of Cytochrome P450: Which Is the Better Oxidant?[†]

Cristina S. Porro, Michael J. Sutcliffe, and Sam P. de Visser*

The Manchester Interdisciplinary Biocenter and the School of Chemical Engineering and Analytical Science,
The University of Manchester, 131 Princess Street, Manchester M1 7DN, United Kingdom

Received: March 17, 2009; Revised Manuscript Received: May 19, 2009

The cytochromes P450 are ubiquitous enzymes that are involved in key metabolizing processes in the body through the monooxygenation of substrates; however, their active oxidant is elusive. There have been reports that implicate that two oxidants, namely, the iron(IV)–oxo porphyrin cation radical (compound I) and the iron(III)–hydroperoxo complex (compound 0), both act as oxidants of sulfoxidation reactions, which contrasts theoretical studies on alkene epoxidation by compounds I and 0 that implicated compound 0 as a sluggish oxidant. To resolve this controversy and to establish the potency of compound I and compound 0 in sulfoxidation reactions, we have studied dimethyl sulfide sulfoxidation by both oxidants using the quantum mechanics/molecular mechanics (QM/MM) technique on cytochrome P450 enzymes and have set up a model of two P450 isozymes: P450_{cam} and P450_{BM3}. The calculations support earlier gas-phase density functional theory modeling and show that compound 0 is a sluggish oxidant that is unable to compete with compound I. Furthermore, compound I is shown to react with dimethyl sulfide via single-state reactivity on a dominant quartet spin state surface.

Introduction

The cytochromes P450 (P450s) are key drug and xenobiotic metabolizing enzymes that because of their broad substrate range and versatility have attracted wide attention.¹ These enzymes utilize molecular oxygen on a heme center and transfer one of those oxygen atoms to a substrate (monooxygenation) to give hydroxylated products, epoxides, or sulfoxides.² Despite immense experimental efforts in the field, the key oxidizing species of the enzyme has still not been unambiguously determined. Possible candidates put forward as the active oxidant in P450 enzymes are the iron(IV)oxo heme($+ \cdot$) species (compound I, Cpd I) and the ferric–hydroperoxo complex (compound 0, Cpd 0).³ There have been suggestions that these two species act side by side as two oxidants. An alternative hypothesis is the two-state reactivity (TSR) scenario where a single oxidant appears in two close lying spin states that masquerade as two oxidants.⁴ This controversy has attracted much attention, but despite many experimental and theoretical studies, it has still not been resolved. A detailed overview of the pros and cons of the two-oxidant versus TSR scenarios is given in recent commentaries.⁵

The active sites of two well-studied P450 enzymes, P450_{cam}⁶ and P450_{BM3}⁷, are shown in Figure 1. P450_{cam} is a bacterial enzyme found in *E. coli* that regioselectively hydroxylates camphor at the C₅ position,⁸ whereas P450_{BM3} is a fatty acid hydroxylase found in *Bacillus megaterium*.⁹ P450_{BM3} resembles the structure and function of eukaryotic P450s closely and as such is a popular target of biochemical studies. Both of these P450s (Figure 1) have a similar active-site structure with a central heme that binds a metal ion (iron), which is linked to the protein backbone through a thiolate bridge of a cysteinate residue: the axial ligand.¹⁰ Molecular oxygen binds to the distal site of the heme (empty in both structures) and in its vicinity the substrate: camphor in P450_{cam} and *N*-palmitoylglycine in

P450_{BM3}. The size and shape of the substrate binding pocket together with the entrance channels leading to the active site determine what substrates are able to bind and eventually react with the active species.

The P450 enzymes undergo a catalytic cycle that is schematically depicted in Scheme 1.^{4b} The cycle starts from the resting state, where a water molecule occupies the distal binding site of the heme (**A**). Upon the entrance of the substrate (SubH) into the active site binding pocket, a spin state crossing from low spin (doublet) to high spin (sextet) is triggered that releases the water molecule from the sixth binding site (**B**). (Also see Figure 1.)¹¹ The heme is reduced (**C**) and binds molecular oxygen (**D**), followed by a second reduction step to form the ferric–peroxy complex (**E**).¹² This process is sufficiently fast that the catalytic cycle enters a gray zone where intermediates are short-lived and information is limited. It has been hypothesized that a protonation step converts **E** into the ferric–hydroperoxo complex (Cpd 0) and a second protonation converts to Cpd I. Low-temperature EPR/ENDOR and resonance Raman studies characterized Cpd 0 as the last stable structure prior to product formation.¹³ Indirect evidence from product distributions and kinetic isotope effect studies, however, assigned the iron(IV)–oxo heme($+ \cdot$), or Cpd I, as the active oxidant of the enzymes.¹⁴

However, this conclusion was put in doubt by site-directed mutagenesis studies, in particular, mutation of Thr₂₅₂ to alanine in P450_{cam},¹⁵ where a regioselectivity switch of hydroxylation to epoxidation was observed in systems where these reactions are competitive.¹⁶ It was therefore concluded that epoxidation reactions originate from Cpd 0, whereas hydroxylation reactions originate from Cpd I and hence a two-oxidant mechanism. Further support for this came from studies on radical clock substrates that gave ultrashort lifetimes of radicals and thereby implicated the activity of two oxidants in the reaction mixture.¹⁷ More recent studies on alkyl sulfide sulfoxidation by P450_{cam} and P450_{BM3} as well as on active site mutants seemed to imply

[†] Part of the “Walter Thiel Festschrift”.

* Corresponding author. E-mail: sam.devisser@manchester.ac.uk.

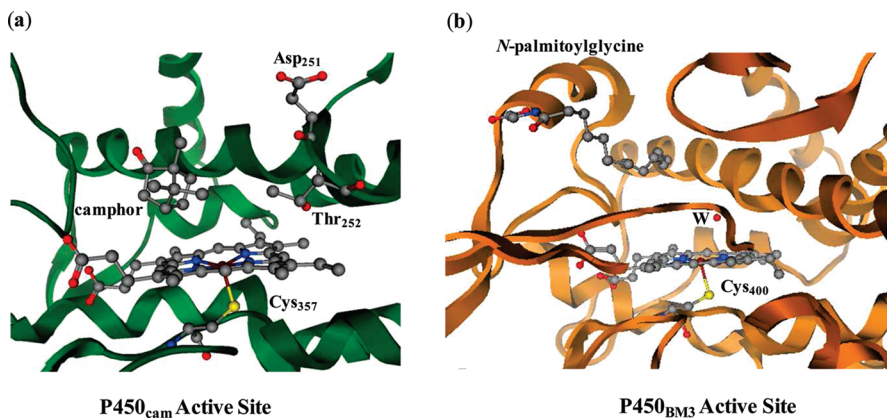
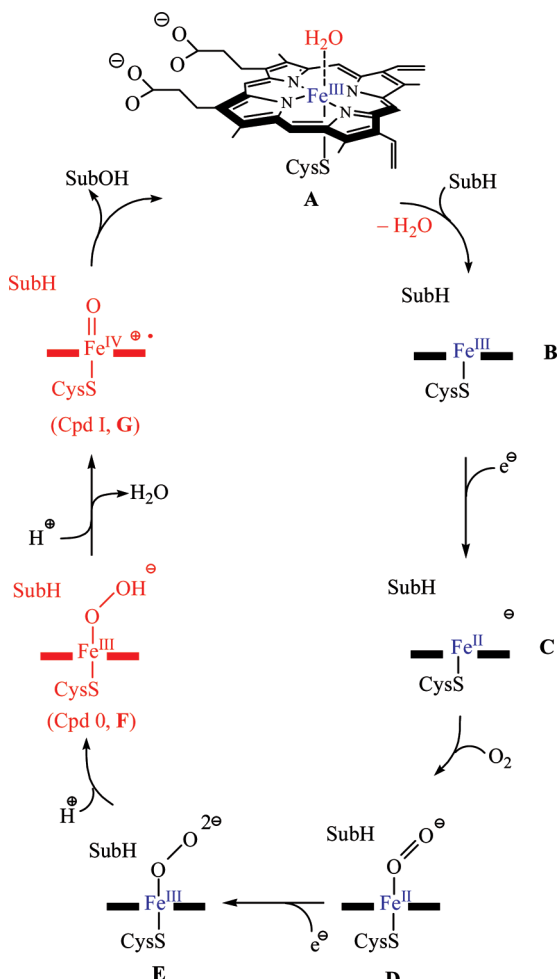


Figure 1. Extracts of the active site of P450_{cam} and P450_{BM3}, as taken from protein data bank files (1DZ4⁶ and 1JPZ,⁷ respectively). Residue numbering corresponds to the respective PDB files, and W represents water molecules.

SCHEME 1: Catalytic Cycle of P450 Enzymes with Cpd I and Cpd 0 Highlighted in Red^a



^a For simplicity, the heme is abbreviated by two horizontal bold bars and cysteinate to CysS.

that Cpd 0 is also a possible oxidant of sulfoxidation reactions.¹⁸ In contrast, other studies of the same group on fatty acid hydroxylation by P450_{BM3} implicated no involvement of Cpd 0, and all reactivity was assigned as originating from Cpd I.¹⁹ The studies with mutant enzymes therefore implicate Cpd 0 in catalyzing sulfoxidation and epoxidation reactions but not hydroxylation reactions.

The two oxidant hypothesis is disputed by density functional theory (DFT) studies on substrate epoxidation by Cpd 0 versus

Cpd I models that showed Cpd 0 to be a sluggish oxidant that is unable to compete with Cpd I.²⁰ These studies showed that Cpd I appears in close-lying doublet and quartet spin states, and in a reaction with substrates, each spin state has a different reaction barrier leading to products and hence TSR. It has been proposed that this TSR phenomenon may masquerade the appearance of two oxidants in reaction mechanisms. Biomimetic studies on model complexes confirmed the theoretical conclusions and proved that the ferric–hydroperoxy complex is unlikely to be an active oxidant of C=C epoxidation reactions.²¹ The question that remains, however, is whether Cpd 0 is able to perform sulfoxidation reactions either in tandem with Cpd I or as the sole oxidant. Earlier DFT studies on small model complexes seemed to imply that Cpd 0 is a sluggish oxidant in sulfoxidation reactions that is unable to compete with Cpd I.^{22,23} These studies, however, did not take the protein environment of the enzyme into account and may not have been a good representative of an enzymatic reaction mechanism. In particular, quantum mechanics/molecular mechanics (QM/MM) studies of Thiel et al.²⁴ on Cpd I of P450_{cam} showed large differences between gas-phase DFT models and QM/MM because of the effect of hydrogen bonding and the protein environment. Importantly, the electronic description of Cpd I appears to be sensitive to interactions of hydrogen bonding donors toward the thiolate, and as a consequence, the system changes from a cysteinyl radical in the gas-phase to a heme radical in an enzyme-mimicked environment, which has been termed “chameonic behavior”.²⁵ The questions addressed in this work are therefore: (a) is the sulfoxidation reaction in P450 enzymes catalyzed by Cpd 0, Cpd I, or both; (b) are different oxidants or multiple spin states active; and (c) what is the effect of the protein environment on substrate sulfoxidation?

Despite the fact that experimental product distributions with WT versus mutant enzymes seemed to implicate a two-oxidant scenario, there are also experimental studies that favor the TSR scenario. Experimental product distributions of rearranged and nonrearranged reaction products proved that substrate hydroxylation proceeds via a radical mechanism and that no cations are involved, which is supportive of the TSR scenario.²⁶ Furthermore, kinetic isotope effect studies on N-dealkylation reactions by P450_{cam} found no evidence of Cpd 0 activity, and all reactivities were assigned to Cpd I.²⁷ Crystallographic data on WT and T252A and D251N mutants of P450_{cam} showed that Thr is not involved in the proton transfer processes during oxygen activation in the catalytic cycle, but instead, the studies showed that the Thr residue is important in hydrogen bonding interactions with the ferric–hydroperoxy complex to facilitate

a fast proton transfer to form Cpd I. The crystallography studies identified several crystal water molecules that remained in the active site pocket of the T252A mutant and would be able to take over the proton-relay function in the mutant, so that Cpd I formation is more likely slowed down rather than hampered.²⁸ The enzyme P450_{eryF} has an unusual P450 active site structure because it lacks this active site Thr residue but instead has an alanine group in its position. However, crystal structure studies showed that the 5-OH group of its natural substrate, 6-deoxyerythronolide B, replaces the function of the Thr group by shuttling protons to and from the heme center.²⁹

In this work, we present the first QM/MM set of calculations on the sulfoxidation reaction by Cpd 0 and Cpd I of two P450 model systems, namely, P450_{cam} and P450_{BM3}. Our calculations confirm DFT studies of small model complexes^{22,23} and show that Cpd 0 is a sluggish oxidant that is unable to compete with Cpd I.

Methods

Quantum Mechanics/Molecular Mechanics Calculations. The QM/MM calculations were performed with the ONIOM program³⁰ as implemented in Gaussian 03.³¹ ONIOM employs the link atoms procedure to treat the boundary region between the QM and MM subsystems, where a covalent bond between the QM and MM regions is replaced by a C–H bond.³² The universal force field (UFF)³³ was selected to compute the MM region, whereas the QM region was treated with DFT. QM/MM test calculations that employed an Amber force field reproduced the calculated electronic states of Cpd I using the UFF force field perfectly so that we do not expect major differences upon changing the MM force field here. Moreover, QM/MM studies using the UFF force field as a description of the MM region were shown to give good geometries and able to predict spectroscopic parameters excellently.^{34,35} We use default QM/MM settings in ONIOM that include mechanical embedding of the protein in the QM region. Full geometry optimizations were performed on all atoms in the QM and MM regions using the unrestricted open-shell version of the hybrid (HF/DFT) density functional UB3LYP.³⁶ The basis set used in the investigations was LANL2DZ, which includes the Los Alamos effective core potential (ECP) plus double- ζ basis set on the Fe atom combined with 6-31G on the rest of the atoms, basis set B1.³⁷ For selected geometries, additional single-point calculations were performed with a larger basis set including polarization functions on all (non-transition-metal) atoms: LACVP**, basis set B2. In the case of ^{2,4}Cpd I of P450_{cam}, we also did a full QM/MM geometry optimization with B3LYP/LACVP** but found little difference with respect to those obtained with the smaller basis set and hence the rest of the studies used basis set B1 for geometry optimization only.

Set-Up for P450_{cam} System. Model 1 is a QM/MM representation of P450_{cam}, which contains the active center plus a 10 Å radius of the surrounding protein. Starting coordinates for the calculations were taken from monomer A of the protein databank file 1DZ4⁶ (1.6 Å resolution) and the protein truncated at a distance of 10 Å from the iron atom. All amino acid residues with at least one atom within this radius were included, namely, Tyr₇₅, Pro₈₆, Phe₈₇, Tyr₉₆, Phe₉₈, Pro₁₀₀, Thr₁₀₁, Gln₁₀₈, Arg₁₁₂, Val₁₁₉, Leu₂₄₄, Leu₂₄₅, Val₂₄₇, Gly₂₄₈, Gly₂₄₉, Asp₂₅₁, Thr₂₅₂, Val₂₅₃, Phe₂₅₆, Leu₂₈₉, Leu₂₉₄, Val₂₉₅, Asp₂₉₇, Arg₂₉₉, Gln₃₂₂, Thr₃₄₉, Phe₃₅₀, Gly₃₅₁, Ser₃₅₄, His₃₅₅, Leu₃₅₆, Cys₃₅₇, Leu₃₅₈, Gly₃₅₉, Gln₃₆₀, Leu₃₆₂, Ala₃₆₃, Glu₃₆₆, and Ile₃₆₇. The camphor substrate was removed from the PDB file and replaced by dimethyl sulfide (DMS), and hydrogen atoms were added to

the system. Unconventional protonation states for residues are taken from earlier studies on P450_{cam}:^{24a} the carboxylic acid side chain of Glu₃₆₆ was protonated, His₃₅₅ was protonated at both nitrogen atoms, and Asp₂₉₇ was protonated at the OD2 atom.

To model the reactive species, distal ligand groups were replaced by OOH⁻ and O, respectively, to generate starting structures for Cpd 0 and Cpd I. The Cpd 0 system comprised 780 atoms with an overall charge of +1, whereas 769 were included in Cpd I, giving a total charge of +2. To prevent this system from undergoing unnatural changes during the geometry optimizations, all α -carbons in the amino acid residues in the MM region were frozen.

Setup for P450_{BM3} System. Model 2 is a P450_{BM3} model whereby we used the 1.06 Å resolution crystal structure of Leys et al.⁷ Hydrogen atoms were added using the MOE2005.06 program package,³⁸ and the proton assignments for the histidine residues in the system were used as follows: all histidine residues were doubly protonated, except for His₆₆, His₁₂₃, His₂₁₀, and His₂₈₇, which were protonated on the ND1 atom only, and His₃₉₇, which was protonated on the NE2 atom only. DMS was added as a substrate to the binding pocket.

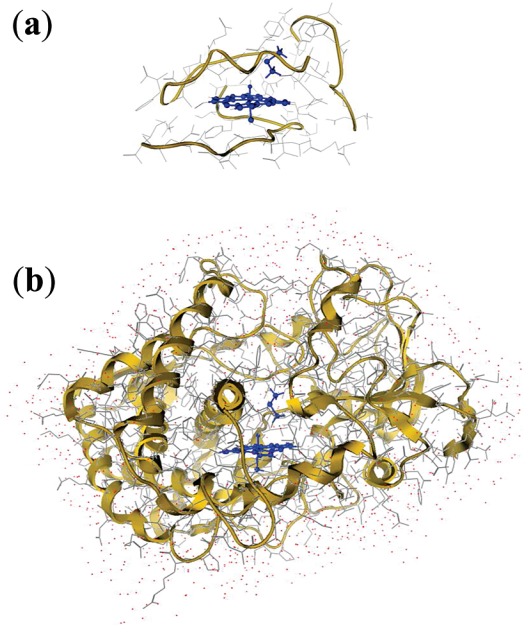
AMBER parameter files for DMS were generated using the Antechamber program within the AMBER software package using the AM1-BCC charge method, whereas heme parameters were taken from the Amber Parameter Database.³⁹ The FF94 force field was used in combination with the GAFF force field for the molecular dynamics (MD) simulations.⁴⁰ Subsequently, the system was solvated in a 15 Å layer of TIP3P water molecules in a truncated octahedral box with a total of about 52 000 atoms and a net charge of -9. The procedure for the equilibration was as follows: (i) an initial minimization with restrained protein and ligand, (ii) an unrestrained minimization, and (iii) a heating stage from 0 to 300 K with restrained ligand and protein. An NVT MD run was performed starting with decreasing levels of restraint until an unrestrained run lasting 400 ps was completed.

Several low-energy structures in the unrestrained MD run were selected as starting points for the QM/MM calculations with snapshots (Sn) taken after 513, 715, and 766 ps. These three starting structures are identified as Sn₁, Sn₂ and Sn₃, respectively. The entire protein was included in the QM/MM calculation as well as a 5 Å layer of water molecules around the surface of the protein. All other water molecules and Na⁺ counterions added by Amber⁴¹ were removed because Gaussian 03 has a limit of about 20 000 atoms.

Model. The QM region in all systems described here included the iron atom, the heme without side chains, thiolate for the cysteinate axial ligand, the distal ligand of the heme and the substrate. It is known that the electronic properties of Cpd I are sensitive to the choice of the axial ligand and its hydrogen bonding interactions with local peptide bonds.^{24,25a,42} To test the effect of the axial ligand description and its hydrogen bonding environment on the obtained calculations, we did further studies with the expanded axial ligand region for selected systems where the axial ligand was expanded to SCH₃⁻, Cys⁻, SH⁻•(HNH₂)₂, and Cys⁻•(HNH₂)₂. (See text for details.) Expansion of the QM system did not affect the electronic description of the various intermediates but did lead to geometric differences. We, therefore, do not expect major changes in the reaction mechanisms and barriers upon enlarging the QM region.

Full geometry optimization of all atoms in the QM and MM regions were performed in C₁ symmetry. Each species was confirmed as a minimum energy structure using an analytical

SCHEME 2: Models of (a) P450_{cam} and (b) P450_{BM3} in This Study with the QM Region Highlighted in Blue



frequency analysis. For the large model, however, frequency calculations were not practical because of the amount of memory needed. Instead, a frequency analysis of the QM region alone was performed using UB3LYP/LANL2DZ in Gaussian 03. We tested two different models (Scheme 2), one based on P450_{cam} and the other based on P450_{BM3}.

Results and Discussion

Cpd I of P450_{cam} and P450_{BM3}. We calculated two models that represent two different P450 enzyme classes: (a) the P450_{cam} model, which is a truncated model that contains the heme and its nearest environment (approximately 10 Å area around the metal) and whereby all α -carbons of the protein are fixed, and (b) the P450_{BM3} model, which contains the complete enzyme plus a solvent layer where no constraints in the chemical system are used. The MD simulation of the latter provided three low-energy snapshots (Sn₁, Sn₂, and Sn₃) taken after 513, 715, and 766 ps. Figure 2 shows optimized geometries of ^{4,2}Cpd I as calculated for P450_{cam} and P450_{BM3}, whereby Cpd I_{cam} represents the P450_{cam} model and Cpd I_{BM3} represents the P450_{BM3} system. In the case of ^{2,4}Cpd I_{cam}, a QM/MM geometry optimization was done with basis set B1 as well as with B2.

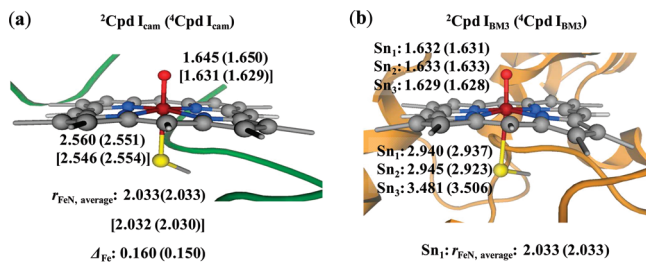


Figure 2. Optimized geometries of Cpd I of (a) P450_{cam} and (b) P450_{BM3} as calculated with QM/MM. Bond lengths are given in angstroms, Δ_{Fe} represents the displacement of the metal from the plane of the heme, and $r_{\text{FeN,average}}$ is the average of the four Fe–N_{pyrrole} distances. Values in square brackets were obtained through optimization with B3LYP/LACVP**.

TABLE 1: Group Spin Densities (ρ) and Fe–S Bond Distances of ²Cpd I of P450_{BM3} with Extended Axial Ligand QM Region

axial ligand	group spin densities						$r_{\text{Fe-S}}$ (Å)
	Fe	O	Por	Cys	DMS	(HN) ₂	
SH [−] (Sn ₁)	1.21	0.89	−0.38	−0.72	0.00		2.940
SH [−] (Sn ₂)	1.20	0.90	−0.36	−0.74	0.00		2.945
SH [−] (Sn ₃)	1.21	0.87	−0.21	−0.87	0.00		3.481
SCH ₃ [−]	1.16	0.93	−0.27	−0.82	0.00		2.670
Cys [−]	1.18	0.91	−0.31	−0.78	0.00		2.701
SH [−] –(HN) ₂	1.19	0.90	−0.31	−0.70	0.00	−0.08	2.988
Cys [−] –(HN) ₂	1.12	0.98	−0.37	−0.73	0.00	0.00	2.505

As follows from the comparative geometries in Figure 2, polarization functions give minor changes in geometry; therefore, we continued the rest of the studies with basis set B1 for geometry optimization and did single-point calculations with basis set B2 only.

Cpd I has close-lying doublet and quartet spin states, each with three unpaired electrons, and as a consequence, TSR patterns are expected on competing spin state surfaces.⁴ The spin multiplicity is identified here with a superscript in the label. Therefore, Cpd I is a triradicaloid with two unpaired electrons triplet coupled in orthogonal π^*_{FeO} orbitals and a third unpaired electron on the heme.⁴³ The latter orbital in D_{4h} symmetry has the label a_{2u} , and we will keep this nomenclature here for simplicity. The a_{2u} orbital shows significant mixing of the heme with a π_S orbital on the axial ligand, and it has been shown that perturbations due to the protein environment, that is, as a result of hydrogen bonding interactions toward thiolate, influence the heme radical character.^{25,44}

As follows from the optimized geometries of ^{4,2}Cpd I of P450_{cam} and P450_{BM3} shown in Figure 2, the environment around the active site is seen to influence the geometry of the active species considerably. Notably, Cpd I of P450_{BM3} has a longer Fe–S bond length, whereas the Fe–O and Fe–N distances are similar to those in P450_{cam}. We tested calculations using three different snapshots from the MD simulations, which had starting distances for the Fe–S bond of 3.00, 2.65, and 3.23 Å, respectively, for Sn₁, Sn₂ and Sn₃. Snapshot Sn₂, however, converged to a geometry similar to that found for Sn₁ with an optimized Fe–S distance of 2.945 (2.923) Å for ²Cpd I_{BM3} (⁴Cpd I_{BM3}), respectively. It appears, therefore, that the long Fe–S distance is inherent to the model of the P450_{BM3} complex.

To test whether the differences in geometry and, in particular, the long Fe–S distances obtained for the P450_{BM3} model influence the reaction mechanisms and electronic configuration of the intermediates, we did some extra calculations where we extended the QM region to take the features of the axial ligand and its direct environment into account. Previous studies using DFT modeling as well as QM/MM showed that the group spin densities are sensitive to the environment of the axial ligand and can change the electronic situation from a dominant thiolate radical (Por Cys[−]) to a porphyrin cation radical (Por⁺ Cys[−]).^{24,25} It was shown that these two configurations are close in energy in Cpd I and that the two valence bond states mix. The amount of mixing thereby gives rise to the large variation in group spin densities. First, starting from Sn₁ optimized geometry, we extended the description of the cysteinate ligand to methylmercaptane (CH₃S[−]) and cysteinate (Cys[−]), and in a second set of calculations, we also included two hydrogen bonded amide groups that form hydrogen bonding interactions with the thiolate ligand. Full geometry optimization of ²Cpd I of P450_{BM3} with

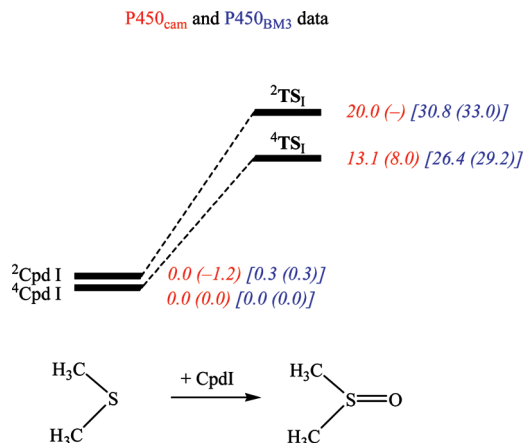


Figure 3. Potential energy profile for the sulfoxidation of DMS by Cpd I of P450_{cam} (in red) and P450_{BM3} (in blue). Energies are in kilocalories per mole relative to the reactant complex in the quartet spin state and contain zero-point corrections. All data were obtained with basis set B1, whereas data in parentheses for P450_{cam} use energies calculated with basis set B2.

extended QM region was performed, and the group spin densities and key bond lengths of the optimized geometries are displayed in Table 1. However, as follows from Table 1, the group spin densities of our P450_{BM3} model shows little sensitivity to the choice of the QM region. Optimized geometries, by contrast, give some fluctuation of the Fe–S distance, which is long when thiolate is chosen as the axial ligand but drops to 2.505 Å for the full cysteinate with hydrogen bonding interactions included. Therefore, the results in Table 1 imply that the long Fe–S distances calculated for the P450_{BM3} models will not influence the electronic properties of Cpd I and consequently should give the correct electronic configuration and barrier heights for the reaction mechanism. Alternative calculations that started from different MD snapshots, one with a larger Fe–S distance in the starting structure and one with a shorter one, converged to similar optimized geometries and virtually identical group spin densities. As a matter of fact, the porphyrin spin density for Sn₁ with SH[−] is almost identical to that found for the system with the large axial ligand description, which implies that Sn₁ with thiolate ligand is a good model of Cpd I despite the long Fe–S distance.

The large amount of cysteinate spin density obtained for ^{4,2}Cpd I of P450_{BM3} is, therefore, not the result of choice of the QM region, although the Fe–S distance shortens when a larger axial ligand system is considered. Because the group spin densities stay the same for all structures considered in Table 1, it is not expected that the long Fe–S distances in P450_{BM3} influence the reaction barriers of sulfoxidation.

Sulfoxidation by Cpd I of P450_{cam} and P450_{BM3}. Subsequently, we studied DMS sulfoxidation by our P450_{cam} and P450_{BM3} (Sn₁) models. The sulfoxidation reaction of DMS by Cpd I of P450 is a concerted reaction via a transition state (TS₁) leading to sulfoxide product complexes (P). Figure 3 shows the potential energy profile of DMS sulfoxidation by P450_{cam} and P450_{BM3} as obtained from QM/MM modeling. Although the doublet and quartet spin states are degenerate for Cpd I, in the transition states, the quartet spin state is lower in energy than the doublet by 6.9 kcal mol^{−1} for P450_{cam} and 4.4 kcal mol^{−1} for P450_{BM3}. These relative energies and spin-state ordering closely match those obtained by small DFT model complexes,^{22,23} although another recent DFT study predicted a lower-lying doublet mechanism.^{45,46} Nevertheless, all previous studies, in

TABLE 2: DMS Sulfoxidation Barriers (ΔE^\ddagger) by Cpd I of P450 As Calculated with Gas-Phase DFT Models or QM/MM Methods on Enzymatic Systems

QM method	DFT or QM/MM	ΔE^\ddagger ^a	ref
UB3LYP/LACVP**	DFT	16.8 (19.2) ^b	22
UB3LYP/LACV3P++**//LACVP**	DFT	11.4 (6.9) ^{b,c}	46
UB3LYP/LACV3P++**//LACVP**+ZPE	DFT	9.1 (7.1) ^c	46
UB3LYP	DFT	20.6 (17.4)	45
UB3LYP/B1, P450 _{cam}	QM/MM	14.4 (21.6)	this work
UB3LYP/B1+ZPE, P450 _{cam}	QM/MM	13.1 (20.0)	this work
UB3LYP/B2//B1+ZPE, P450 _{cam}	QM/MM	8.0	this work
UB3LYP/B1, P450 _{BM3}	QM/MM	26.4 (30.8)	this work
UB3LYP/B1+ZPE, P450 _{BM3}	QM/MM	29.2 (33.0)	this work

^a In kilocalories per mole; values in parentheses for the doublet spin state. ^b Without ZPE correction. ^c Including environmental perturbations ($\epsilon = 5.7$) and hydrogen bonding interactions toward thiolate.

accord with the current study, predict a single-state reactivity (SSR) mechanism whereby one spin-state surface is dominant.

Because the absolute barriers appear to give a large deviation based on the method and model chosen, we summarize relative energies and barrier heights obtained in this work and how they compare with the literature in Table 2. Therefore, the DFT model calculations of refs 22, 23, 45, and 46 use an active site representation of a P450 enzyme that contains protoporphyrin IX bound to an oxo group and a cysteinate mimic that is represented by either thiolate (SH[−]) or methylmercaptane (SCH₃[−]). These calculations were done in the gas phase, and the effect of the protein environment of the enzyme is neglected. Some studies report additional continuum solvent calculations^{47–49} that mimic environmental effects on the charge and spin distributions of the structures to mimic the effect of the surrounding.

As can be seen from Table 2, there is a large range of calculated sulfoxidation barriers for seemingly the same model. All methods predict high ΔE values when using a small basis set, with barriers well over 20 kcal mol^{−1} in some cases. The addition of ZPE corrections to the relative energies typically changes the barriers by maximally a few kilocalories per mole but does not change the doublet/quartet spin-state ordering. Further corrections to the relative energies with an improved basis set leads to significantly lower barriers, which again is seen with QM/MM and gas-phase DFT calculations. The value of ⁴TS₁ of P450_{cam} with the large basis set and ZPE corrections included is 8.0 kcal mol^{−1} above reactants, which compares very well with the value obtained with a small DFT model where 9.1 kcal mol^{−1} was calculated with comparable methods and basis sets. All studies predict single-state reactivity (SSR) patterns on one dominant spin state surface. The gas-phase DFT models seem to imply a lower-lying doublet spin state surface, at least without ZPE corrections included. Our QM/MM studies on both P450_{cam} and P450_{BM3} predict a lower quartet spin state surface by at least 3.8 kcal mol^{−1}.

Although the sulfoxidation mechanism shows an SSR scenario, this is different from aliphatic hydroxylation reactions catalyzed by P450 enzymes, where TSR is usually found with similar reaction barriers on the two spin state surfaces.⁴⁷ Moreover, aliphatic hydroxylation proceeds in a stepwise manner with an initial hydrogen abstraction followed by radical rebound.^{42,47,48} This radical intermediate, because of its finite lifetime, can lead to rearrangement and the formation of

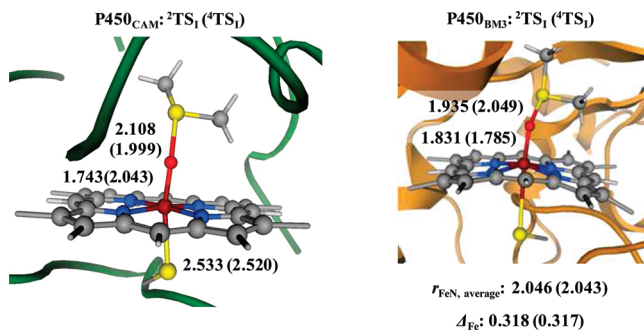


Figure 4. Optimized geometries of ${}^4,2\text{TS}_1$ of $\text{P}450_{\text{cam}}$ and $\text{P}450_{\text{BM}3}$, as obtained from QM/MM with bond lengths given in angstroms. The displacement of the metal from the heme plane is estimated to be Δ_{Fe} , and $r_{\text{FeN}, \text{average}}$ is the average value of the four $\text{Fe}-\text{N}_{\text{pyrrole}}$ distances.

byproduct in the reaction mechanism.⁴⁹ Sulfoxidation, by contrast, is not expected to give byproduct. In summary, although at first glance the relative energies obtained with QM/MM are seemingly very different from gas-phase DFT models, the barrier heights are, in fact, sensitive to basis set and zero-point corrections. Including these effects in the calculations predicts similar reaction energies and reaction mechanisms as compared with those obtained with small model (gas-phase) complexes. It is currently unclear what the origin of the high barriers for $\text{P}450_{\text{BM}3}$ is.

The potential energy profiles of the sulfoxidation of DMS by Cpd I of $\text{P}450_{\text{cam}}$ differs somewhat from that for $\text{P}450_{\text{BM}3}$ (Figure 3). The geometric differences obtained and why that leads to energy differences are discussed below. Optimized geometries of ${}^4,2\text{TS}_1$ of $\text{P}450_{\text{cam}}$ and $\text{P}450_{\text{BM}3}$ are shown in Figure 4. The two $\text{P}450_{\text{cam}}$ transition states are found to have similar geometrical characteristics, although the low-spin structure has an S–O distance that is 0.1 Å longer than that obtained for the high-spin state. The Fe–O distance is elongated in the high spin state, reaching over 2.0 Å, whereas in the low spin state, it is much shorter: 1.74 Å. These differences are the result of differences in molecular orbital occupation. Therefore, occupation of the σ_{z2}^* orbital with one electron in ${}^4\text{TS}_1$ increases the antibonding character of the Fe–O and Fe–S bonds, hence producing elongated bond lengths. The angle between Fe, O, and the DMS sulfur atom is approximately 150°. In addition to the truncated model of $\text{P}450_{\text{cam}}$, we also performed a full QM/MM calculation on the full enzyme (Sn_1 of $\text{P}450_{\text{BM}3}$). These studies were done to establish the effect of the environment because of the size of the MM region on the sulfoxidation reaction. Moreover, $\text{P}450_{\text{cam}}$ and $\text{P}450_{\text{BM}3}$ have different structural features that may determine the reactivity differences.

The ${}^2\text{TS}_1$ structures obtained for $\text{P}450_{\text{cam}}$ and $\text{P}450_{\text{BM}3}$ have geometric features that are similar to those of the new transition state of Shaik et al.⁴⁶ with a large $\text{Fe}-\text{O}-\text{SDMS}$ angle of 150.8 and 174.0° for $\text{P}450_{\text{cam}}$ and $\text{P}450_{\text{BM}3}$, respectively. Our obtained transition state, however, is much later on the potential energy profile with long Fe–O and O–S distances compared with the structure found with the small DFT model. Obviously, the protein environment influences the structure of the transition state considerably and changes it to a later position on the potential energy surface. Consequently, the barrier is also increased with respect to the small DFT model. As a result of the large differences in molecular geometries for ${}^2\text{TS}_1$, also widely diverging values for the imaginary frequency are obtained ranging from $i61.1^{45}$ to $i291.9 \text{ cm}^{-1}$.⁴⁶ In our study, imaginary frequencies of $i212.2$ and $i383.6 \text{ cm}^{-1}$ for the low-spin and high-spin transition states in $\text{P}450_{\text{cam}}$, respectively, were

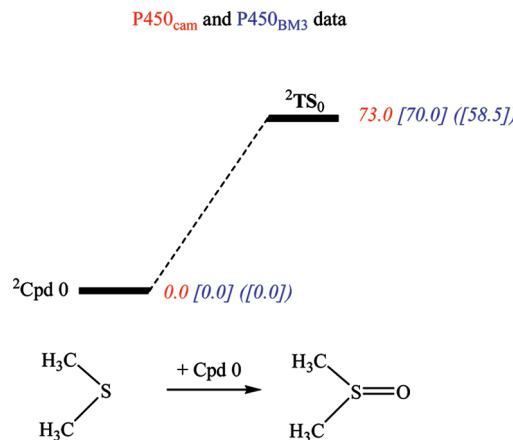


Figure 5. Potential energy profile for the sulfoxidation of DMS by Cpd I of $\text{P}450_{\text{cam}}$ (in red) and $\text{P}450_{\text{BM}3}$ (in blue). All energies are in kilocalories per mole relative to the reactant complex in the doublet spin state and contain zero-point corrections. Data out of parentheses and in square brackets were obtained with basis set B1, whereas data in parentheses were obtained with basis set B2.

obtained. The transition states in $\text{P}450_{\text{BM}3}$, on the other hand, are characterized by a single imaginary frequency of $i276 \text{ cm}^{-1}$ for the low-spin and $i147 \text{ cm}^{-1}$ for the high-spin species. All sulfoxidation imaginary frequencies described in this work correspond to an S–O stretch vibration indicative of a bond formation process. A somewhat larger value for the imaginary frequency for the high-spin transition state is reported from gas-phase DFT studies with values of $i680.6$,²² $i689.2$,⁴⁶ and $i697.8 \text{ cm}^{-1}$,⁴⁵ respectively. Geometrically, these ${}^4\text{TS}_1$ transition states are very much alike and also resemble the structure shown above in Figure 4.

From the structures shown in Figure 4, it is clear that the two $\text{P}450_{\text{BM}3}$ transition states are similar in geometry. The largest difference between ${}^4,2\text{TS}_1$ obtained is for the S–O distance with a short bond length of 1.935 Å for ${}^2\text{TS}_1$ and 2.049 Å for ${}^4\text{TS}_1$. These distances occur at much shorter S–O distance than that in $\text{P}450_{\text{cam}}$. In the transition state, the Fe–O distance is slightly elongated compared with Cpd I with values of 1.831 and 1.785 Å for the low and high spin states, respectively.

Optimized geometries calculated with QM/MM compare well to earlier obtained structures, even though those studies ignored the protein surrounding. Therefore, QM/MM supports the recent assignment⁴⁶ of the low-spin structure (${}^2\text{TS}_1$) as an upright configuration rather than the bend configuration reported in ref 22. As a consequence, the ${}^4\text{TS}_1$ and ${}^2\text{TS}_1$ structures obtained here are close in geometry; in particular, the Fe–S distances are within 0.033 Å. The Fe–O and O–S distances in ${}^4\text{TS}_1$ of $\text{P}450_{\text{BM}3}$ are close to those obtained with small DFT model complexes from refs 22, 45, and 46, where values of 1.767, 1.804, and 1.769 Å (for the Fe–O distance) and values of 2.032, 2.012, and 2.028 Å (for the O–S distance) were reported, respectively. Although, the Fe–S and O–S distances for ${}^4\text{TS}_1$ in $\text{P}450_{\text{cam}}$ are similar to these values, a much longer Fe–O distance of 2.034 Å is found. Moreover, the vibrational mode in the transition state is one for an S–O bond stretching mode and therefore is a motion leading to sulfoxide products. Therefore, it follows from the calculations presented here and those in the literature that calculations on a sulfoxidation reaction by an iron(IV)–oxo species are sensitive to environmental perturbations so that the choice and shape of the model may dramatically influence reaction barriers.

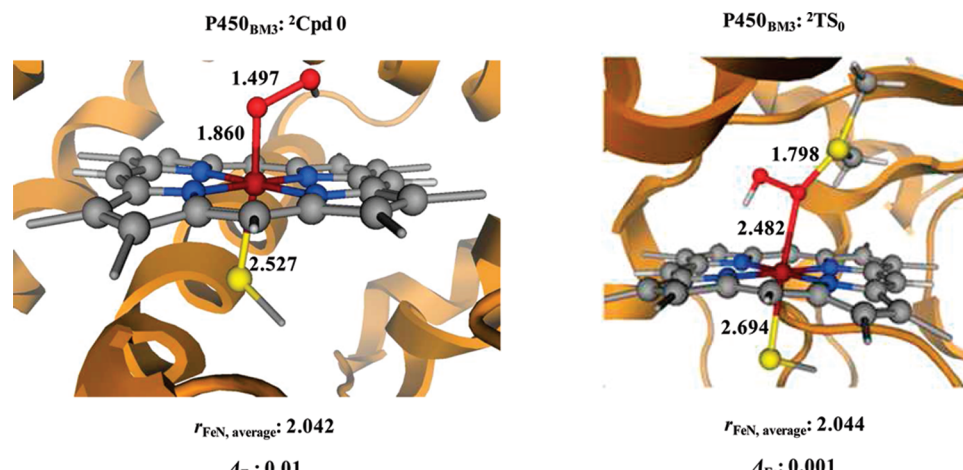


Figure 6. Optimized geometries of $^2\text{Cpd}\ 0$ and $^2\text{TS}_0$ of $\text{P}450_{\text{BM}3}$ as obtained from QM/MM with bond lengths given in angstroms. The average Fe—N_{pyrrole} distance is given as $r_{\text{FeN,average}}$, and Δ_{Fe} is the displacement of the metal from the plane of the heme.

Sulfoxidation of Dimethyl Sulfide by Cpd 0 of $\text{P}450_{\text{cam}}$ and $\text{P}450_{\text{BM}3}$. Experimental studies^{16–18} seemed to suggest that there are two oxidants active in P450 enzymes, which have been assigned as Cpd I and Cpd 0. Mutation studies that should prevent one protonation mechanism in the catalytic cycle of P450, for example, T252A in $\text{P}450_{\text{cam}}$, are expected to stop the catalytic cycle with the ferric–hydroperoxy species, that is, Cpd 0. These mutants still gave sulfoxidation products, albeit with much smaller rate constants than WT enzyme.¹⁸ To study whether Cpd 0 would be active in either $\text{P}450_{\text{cam}}$ or $\text{P}450_{\text{BM}3}$, we set up QM/MM models of Cpd 0 of these enzyme structures similarly to those discussed above for Cpd I reactivity.

The potential energy profile of the reaction of Cpd 0 with DMS leading to dimethyl sulfoxide products is shown in Figure 5. Similar to the reaction of Cpd I with DMS, with Cpd 0, a concerted reaction mechanism is obtained via a single transition state (TS_0). However, the electronic ground state of Cpd 0 is a doublet spin state that is well separated from the quartet and sextet spin states.²⁰ As such, Cpd 0 reacts with substrates via SSR on a dominant doublet spin state surface. The reaction barriers for DMS sulfoxidation by Cpd 0 are extremely high (Figure 5), much higher than barriers typically expected in an enzymatic system and quite higher than those obtained for Cpd I, even for the $\text{P}450_{\text{BM}3}$ system with the elevated sulfoxidation barriers. Therefore, with reaction barriers well over 50 kcal mol⁻¹, it is unlikely that Cpd 0 will be able to react with sulfides via sulfoxidation reactions. These studies are in line with previous theoretical reports where the reaction barriers starting from Cpd 0 were found to be at least double the height of those for Cpd I.^{22,23} The reaction energies for our $\text{P}450_{\text{cam}}$ and $\text{P}450_{\text{BM}3}$ models are very close and indicate that the effect of the protein environment on the reaction is very small.

Optimized geometries of $^2\text{Cpd}\ 0$ and $^2\text{TS}_0$ for $\text{P}450_{\text{BM}3}$ are given in Figure 6. In the transition state, the S—O distance is relatively short (1.798 Å), which is much shorter than the distance found for $^2\text{TS}_1$. (See Figure 4.) At this point, the Fe—O distance is elongated to 2.482 Å, clearly showing weakening of the Fe—O bond.

In summary, QM/MM studies show that the sulfoxidation of dimethyl sulfide proceeds via Cpd I because Cpd 0 is a sluggish oxidant that is unable to compete with Cpd I. These studies support previous DFT studies on alkyl sulfide sulfoxidation mechanisms but take a key factor into effect that was neglected before, namely, the protein environment.

Summary and Conclusions

We report the first QM/MM study on sulfoxidation by Cpd 0 and Cpd I of P450 enzymes. Our calculations support previous studies in the field using small DFT models, namely, Cpd I is the sole oxidant of P450 enzymes. Cpd 0 gives very high reaction barriers for substrate sulfoxidation and will be unable to compete with the much lower barriers obtained for Cpd I. Although Cpd I appears in two close-lying spin states (doublet and quartet), only the quartet spin state is found to be active, so the system will react via SSR.

Acknowledgment. The research was supported by a studentship to C.S.P. from a Doctoral Training Award (DTA) of the Engineering and Physical Sciences Research Council (EPSRC, U.K.). In addition, research grant funding from the Biotechnology and Biological Sciences Research Council (BBSRC U.K., grant code BB/F002521/1 and BB/C511305/1) is acknowledged.

Supporting Information Available: Cartesian coordinates of all structures described in this work as well as absolute energies and group spin densities. This material is available free of charge via the Internet at <http://pubs.acs.org>.

References and Notes

- (a) Guengerich, F. P. *Chem. Res. Toxicol.* **2001**, *14*, 611–650. (b) *Cytochrome P450: Structure, Mechanism, and Biochemistry*, 3rd ed.; Ortiz de Montellano, P. R., Ed.; Kluwer Academic/Plenum Publishers: New York, 2004. (c) Munro, A. W.; Girvan, H. M.; McLean, K. J. *Nat. Prod. Rep.* **2007**, *24*, 585–609.
- (a) Sono, M.; Roach, M. P.; Coulter, E. D.; Dawson, J. H. *Chem. Rev.* **1996**, *96*, 2841–2888. (b) Groves, J. T. *Proc. Natl. Acad. Sci. U.S.A.* **2003**, *100*, 3569–3574.
- Newcomb, M.; Toy, P. H. *Acc. Chem. Res.* **2000**, *33*, 449–455.
- (a) Shaik, S.; de Visser, S. P.; Ogliaro, F.; Schwarz, H.; Schröder, D. *Curr. Opin. Chem. Biol.* **2002**, *6*, 556–567. (b) Shaik, S.; Kumar, D.; de Visser, S. P.; Altun, A.; Thiel, W. *Chem. Rev.* **2005**, *105*, 2279–2328.
- For an overview on the two-oxidant versus two-state reactivity mechanisms, see: (a) Jin, S.; Bryson, T. A.; Dawson, J. H. *J. Biol. Inorg. Chem.* **2004**, *9*, 644–653. (b) Nam, W.; Ryu, Y. O.; Song, W. J. *J. Biol. Inorg. Chem.* **2004**, *9*, 654–660. (c) Shaik, S.; Hirao, H.; Kumar, D. *Nat. Prod. Rep.* **2007**, *24*, 533–552.
- Schlichting, I.; Berendzen, J.; Chu, K.; Stock, A. M.; Maves, S. A.; Benson, D. E.; Sweet, R. M.; Ringe, D.; Petsko, G. A.; Sligar, S. G. *Science* **2000**, *287*, 1615–1622.
- Leys, D.; Mowat, C. G.; McLean, K. J.; Richmond, A.; Chapman, S. K.; Walkinshaw, M. D.; Munro, A. W. *J. Biol. Chem.* **2003**, *278*, 5141–5147.

- (8) (a) Sligar, S. G.; Gunsalus, I. C. *Proc. Natl. Acad. Sci. U.S.A.* **1976**, *73*, 1078–1082. (b) Poulos, T. L. *Biochem. Biophys. Res. Commun.* **2003**, *312*, 35–39. (c) Kuznetsov, V. Y.; Poulos, T. L.; Sevrioukova, I. F. *Biochemistry* **2006**, *45*, 11934–11944. (d) Purdy, M. M.; Koo, L. S.; Ortiz de Montellano, P. R.; Klimman, J. P. *Biochemistry* **2006**, *45*, 15793–15806.
- (9) See, for example: (a) Ruettinger, R. T.; Wen, L. P.; Fulco, A. J. *J. Biol. Chem.* **1989**, *264*, 10987–10995. (b) Warman, A. J.; Roitel, O.; Neeli, R.; Girvan, H. M.; Seward, H. E.; Murray, S. A.; McLean, K. J.; Joyce, M. G.; Toogood, H.; Holt, R. A.; Leys, D.; Scrutton, N. S.; Munro, A. W. *Biochem. Soc. Trans.* **2005**, *33*, 747–753. (c) Girvan, H. M.; Waltham, T. N.; Neeli, R.; Collins, H. F.; McLean, K. J.; Scrutton, N. S.; Leys, D.; Munro, A. W. *Biochem. Soc. Trans.* **2006**, *34*, 1173–1177.
- (10) Poulos, T. L.; Finzel, B. C.; Howard, A. J. *J. Mol. Biol.* **1987**, *195*, 687–700.
- (11) (a) Sligar, S. G. *Biochemistry* **1976**, *15*, 5399–5406. (b) Auclair, K.; Moënne-Locozzo, P.; Ortiz de Montellano, P. R. *J. Am. Chem. Soc.* **2001**, *123*, 4877–4885.
- (12) (a) Denisov, I. G.; Makris, T. M.; Sligar, S. G.; Schlichting, I. *Chem. Rev.* **2005**, *105*, 2253–2277. (b) Meunier, B.; de Visser, S. P.; Shaik, S. *Chem. Rev.* **2004**, *104*, 3947–3980.
- (13) (a) Davydov, R.; Makris, T. M.; Kofman, V.; Werst, D. E.; Sligar, S. G.; Hoffman, B. M. *J. Am. Chem. Soc.* **2001**, *123*, 1403–1415. (b) Mak, P. J.; Denisov, I. G.; Victoria, D.; Makris, T. M.; Deng, T.; Sligar, S. G.; Kincaid, J. R. *J. Am. Chem. Soc.* **2007**, *129*, 6382–6383.
- (14) (a) Egawa, T.; Shimada, H.; Ishimura, Y. *Biochem. Biophys. Res. Commun.* **1994**, *201*, 1464–1469. (b) Kellner, D. G.; Hung, S. C.; Weiss, K. E.; Sligar, S. G. *J. Biol. Chem.* **2002**, *277*, 9641–9644.
- (15) (a) Raag, R.; Martinis, S. A.; Sligar, S. G.; Poulos, T. L. *Biochemistry* **1991**, *30*, 11420–11429. (b) Davydov, R.; Perera, R.; Jin, S.; Yang, T.-C.; Bryson, T. A.; Sono, M.; Dawson, J. H.; Hoffmann, B. M. *J. Am. Chem. Soc.* **2005**, *127*, 1403–1413. (c) Makris, T. M.; von Koenig, K.; Schlichting, I.; Sligar, S. G. *Biochemistry* **2007**, *46*, 14129–14140.
- (16) Vaz, A. D. N.; McGinnity, D. F.; Coon, M. J. *Proc. Natl. Acad. Sci. U.S.A.* **1998**, *95*, 3555–3560.
- (17) (a) Newcomb, M.; Shen, R.; Choi, S.-Y.; Toy, P. H.; Hollenberg, P. F.; Vaz, A. D. N.; Coon, M. J. *J. Am. Chem. Soc.* **2000**, *122*, 2677–2686. (b) Chandrasena, R. E. P.; Vatsis, K. P.; Coon, M. J.; Hollenberg, P. F.; Newcomb, M. *J. Am. Chem. Soc.* **2004**, *126*, 115–126.
- (18) Cryle, M. J.; De Voss, J. J. *Angew. Chem., Int. Ed.* **2006**, *45*, 8221–8223.
- (19) Cryle, M. J.; De Voss, J. J. *ChemBioChem* **2008**, *9*, 261–266.
- (20) (a) Ogliaro, F.; de Visser, S. P.; Cohen, S.; Sharma, P. K.; Shaik, S. *J. Am. Chem. Soc.* **2002**, *124*, 2806–2817. (b) Kamachi, T.; Shiota, Y.; Ohta, T.; Yoshizawa, K. *Bull. Chem. Soc. Jpn.* **2003**, *76*, 721–732.
- (21) (a) Song, W. J.; Ryu, Y. O.; Song, R.; Nam, W. *J. Biol. Inorg. Chem.* **2005**, *10*, 294–304. (b) Park, M. J.; Lee, J.; Suh, Y.; Kim, J.; Nam, W. *J. Am. Chem. Soc.* **2006**, *128*, 2630–2634.
- (22) Sharma, P. K.; de Visser, S. P.; Shaik, S. *J. Am. Chem. Soc.* **2003**, *125*, 8698–8699.
- (23) Kumar, D.; de Visser, S. P.; Sharma, P. K.; Hirao, H.; Shaik, S. *Biochemistry* **2005**, *44*, 8148–8158.
- (24) (a) Schöneboom, J. C.; Lin, H.; Reuter, N.; Thiel, W.; Cohen, S.; Ogliaro, F.; Shaik, S. *J. Am. Chem. Soc.* **2002**, *124*, 8142–8151. (b) Schöneboom, J. C.; Neese, F.; Thiel, W. *J. Am. Chem. Soc.* **2005**, *127*, 5840–5853.
- (25) (a) Ogliaro, F.; Cohen, S.; de Visser, S. P.; Shaik, S. *J. Am. Chem. Soc.* **2000**, *122*, 12892–12893. (b) Ogliaro, F.; de Visser, S. P.; Groves, J. T.; Shaik, S. *Angew. Chem., Int. Ed.* **2001**, *40*, 2874–2878. (c) de Visser, S. P.; Shaik, S.; Sharma, P. K.; Kumar, D.; Thiel, W. *J. Am. Chem. Soc.* **2003**, *125*, 15779–15788. (d) Bathelt, C. M.; Zurek, J.; Mulholland, A. J.; Harvey, J. N. *J. Am. Chem. Soc.* **2005**, *127*, 12900–12908.
- (26) He, X.; Ortiz de Montellano, P. R. *J. Biol. Chem.* **2004**, *279*, 39479–39484.
- (27) Dowers, T. S.; Rock, D. A.; Rock, D. A.; Jones, J. P. *J. Am. Chem. Soc.* **2004**, *126*, 8868–8869.
- (28) Nagano, S.; Poulos, T. L. *J. Biol. Chem.* **2005**, *280*, 31659–31663.
- (29) Nagano, S.; Cupp-Vickery, J. R.; Poulos, T. L. *J. Biol. Chem.* **2005**, *280*, 22102–22107.
- (30) (a) Maseras, F.; Morokuma, K. *J. Comput. Chem.* **1995**, *16*, 1170–1179. (b) Vreven, T.; Byun, K. S.; Komáromi, I.; Dapprich, S.; Montgomery, J. A., Jr.; Morokuma, K.; Frisch, M. J. *J. Chem. Theory Comput.* **2006**, *2*, 815–826.
- (31) Frisch, M. J.; Trucks, G. W.; Schlegel, H. B.; Scuseria, G. E.; Robb, M. A.; Cheeseman, J. R.; Montgomery, J. A., Jr.; Vreven, T.; Kudin, K. N.; Burant, J. C.; Millam, J. M.; Iyengar, S. S.; Tomasi, J.; Barone, V.; Mennucci, B.; Cossi, M.; Scalmani, G.; Rega, N.; Petersson, G. A.; Nakatsuji, H.; Hada, M.; Ehara, M.; Toyota, K.; Fukuda, R.; Hasegawa, J.; Ishida, M.; Nakajima, T.; Honda, Y.; Kitao, O.; Nakai, N.; Klene, M.; Li, X.; Knox, J. E.; Hratchian, H. P.; Cross, J. B.; Adamo, C.; Jaramillo, J.; Gomperts, R.; Stratmann, R. E.; Yazyev, O.; Austin, A. J.; Cammi, R.; Pomelli, C.; Ochterski, J. W.; Ayala, P. Y.; Morokuma, K.; Voth, G. A.; Salvador, P.; Dannenberg, J. J.; Zakrzewski, V. G.; Dapprich, S.; Daniels, A. D.; Strain, M. C.; Farkas, O.; Malick, D. K.; Rabuck, A. D.; Raghavachari, K.; Foresman, J. B.; Ortiz, J. V.; Cui, Q.; Baboul, A. G.; Clifford, S.; Cioslowski, J.; Stefanov, B. B.; Liu, G.; Liashenko, A.; Piskorz, P.; Komaromi, I.; Martin, R. L.; Fox, D. J.; Keith, T.; Al-Laham, M. A.; Peng, C. Y.; Nanayakkara, A.; Challacombe, M.; Gill, P. M. W.; Johnson, B.; Chen, W.; Wong, M. W.; Gonzalez, C.; Pople, J. A. *Gaussian 03*, revision C.01; Gaussian, Inc.: Wallingford, CT, 2004.
- (32) Singh, U. C.; Kollman, P. A. *J. Comput. Chem.* **1986**, *7*, 718–730.
- (33) Rappé, A. K.; Casewit, C. J.; Colwell, K. S.; Goddard III, W. A.; Skiff, W. M. *J. Am. Chem. Soc.* **1992**, *114*, 10024–10035.
- (34) Barone, V.; Bencini, A.; Cossi, M.; Di Matteo, A.; Mattesini, M.; Totti, F. *J. Am. Chem. Soc.* **1998**, *120*, 7069–7078.
- (35) Godfrey, E.; Porro, C. S.; de Visser, S. P. *J. Phys. Chem. A* **2008**, *112*, 2464–2468.
- (36) (a) Becke, A. D. *J. Chem. Phys.* **1993**, *98*, 5648–5652. (b) Lee, C.; Yang, W.; Parr, R. G. *Phys. Rev. B* **1988**, *37*, 785–789.
- (37) Hay, P. J.; Wadt, W. R. *J. Chem. Phys.* **1985**, *82*, 299–310.
- (38) MOE, version 2005.06; Chemical Computing Group: Montreal, Canada, 2005. <http://www.chemcomp.com/>.
- (39) Cornell, W. D.; Cieplak, P.; Bayly, C. I.; Gould, I. R.; Merz, K. M., Jr.; Ferguson, D. M.; Spellmeyer, D. C.; Fox, T.; Caldwell, J. W.; Kollman, P. A. *J. Am. Chem. Soc.* **1995**, *117*, 5179–5197.
- (40) Wang, J. M.; Wolf, R. M.; Caldwell, J. W.; Kollman, P. A.; Case, D. A. *J. Comput. Chem.* **2006**, *25*, 1157–1174.
- (41) Case, D. A.; Darden, T. A.; Cheatham, T. E., III; Simmerling, C. L.; Wang, J.; Duke, R. E.; Luo, R.; Merz, K. M.; Pearlman, D. A.; Crowley, M.; Walker, R. C.; Zhang, W.; Wang, B.; Hayik, S.; Roitberg, A.; Sebra, G.; Wong, K. F.; Paesani, F.; Wu, X.; Brozell, S.; Tsui, V.; Gohlke, H.; Yang, L.; Tan, C.; Mongan, J.; Hornak, V.; Cui, G.; Beroza, P.; Mathews, D. H.; Schafmeister, C.; Ross, W. S.; Kollman, P. A. *AMBER 9*; University of California: San Francisco, 2006.
- (42) (a) de Visser, S. P. *Chem.-Eur. J.* **2006**, *12*, 8168–8177. (b) de Visser, S. P. *J. Am. Chem. Soc.* **2006**, *128*, 15809–15818. (c) Shaik, S.; de Visser, S. P.; Kumar, D. *J. Am. Chem. Soc.* **2004**, *126*, 11746–11749.
- (43) Green, M. T. *J. Am. Chem. Soc.* **1999**, *121*, 7939–7940.
- (44) Ogliaro, F.; de Visser, S. P.; Cohen, S.; Kaneti, J.; Shaik, S. *ChemBioChem* **2001**, 848–851.
- (45) Rydberg, P.; Ryde, U.; Olsen, L. *J. Chem. Theory Comput.* **2008**, *4*, 1369–1377.
- (46) Li, C.; Zhang, L.; Zhang, C.; Hirao, H.; Wu, W.; Shaik, S. *Angew. Chem., Int. Ed.* **2007**, *46*, 8168–8170, Erratum: *Angew. Chem., Int. Ed.* **2008**, *47*, 8148.
- (47) (a) de Visser, S. P.; Kumar, D.; Cohen, S.; Shacham, R.; Shaik, S. *J. Am. Chem. Soc.* **2004**, *126*, 8362–8363. (b) Shaik, S.; Kumar, D.; de Visser, S. P. *J. Am. Chem. Soc.* **2008**, *130*, 10128–10140. (c) de Visser, S. P.; Tahsini, L.; Nam, W. *Chem. Eur. J.* **2009**, *15*, 5577–5587.
- (48) de Visser, S. P. *J. Am. Chem. Soc.* **2006**, *128*, 9813–9824.
- (49) (a) de Visser, S. P.; Ogliaro, F.; Shaik, S. *Angew. Chem., Int. Ed.* **2001**, *40*, 2874–2876. (b) de Visser, S. P.; Shaik, S. *J. Am. Chem. Soc.* **2003**, *125*, 7413–7424. (c) Kumar, D.; de Visser, S. P.; Shaik, S. *J. Am. Chem. Soc.* **2003**, *125*, 13024–13025. (d) Kumar, D.; de Visser, S. P.; Sharma, P. K.; Cohen, S.; Shaik, S. *J. Am. Chem. Soc.* **2004**, *126*, 1907–1920.